JIMD Reports
DOI 10.1007/8904_2015_491

RESEARCH REPORT

Detailed Biochemical and Bioenergetic Characterization of *FBXL4*-Related Encephalomyopathic Mitochondrial DNA Depletion

Ghadi Antoun • Skye McBride • Jason R. Vanstone • Turaya Naas • Jean Michaud • Stephanie Redpath • Hugh J. McMillan • Jason Brophy • Hussein Daoud • Pranesh Chakraborty • David Dyment • Martin Holcik • Mary-Ellen Harper • Matthew A. Lines

Received: 06 May 2015 / Revised: 24 July 2015 / Accepted: 30 July 2015 / Published online: 25 September 2015

Abstract Mutations of *FBXL4*, which encodes an orphan mitochondrial F-box protein, are a recently identified cause of encephalomyopathic mtDNA depletion. Here, we describe the detailed clinical and biochemical phenotype of a neonate presenting with hyperlactatemia, leukoencephalopathy, arrhythmias, pulmonary hypertension, dysmorphic features, and lymphopenia. Next-generation sequencing in the proband identified a homozygous frameshift, c.1641_1642delTG, in *FBXL4*, with a surrounding block of SNP marker homozygosity identified by microarray. Muscle biopsy showed a paucity of mitochondria with ultrastructural abnormalities, mitochondrial DNA depletion, and profound deficiency of all respiratory chain complexes. Cell-based mitochondrial phenotyping in fibroblasts showed mitochondrial fragmentation, decreased basal and maximal respiration, absence of ATP-linked respiratory and leak capacity, impaired survival under obligate aerobic respiration, and reduced mitochondrial inner membrane potential, with relative sparing of mitochondrial mass. Cultured fibroblasts from the patient exhibited a more oxidized glutathione ratio, consistent with altered cellular redox poise. High-resolution respirometry of permeabilized muscle fibers showed marked deficiency of oxidative phosphorylation using a variety of mitochondrial energy substrates and inhibitors. This constitutes the fourth and most detailed report of *FBXL4* deficiency to date. In light of our patient's clinical findings and genotype (homozygous frameshift), this phenotype likely represents the severe end of the *FBXL4* clinical spectrum.

Communicated by: Shamima Rahman, FRCP, FRCPCH, PhD

Competing interests: None declared

Electronic supplementary material: The online version of this chapter (doi:10.1007/8904_2015_491) contains supplementary material, which is available to authorized users.

G. Antoun · M.-E. Harper
Department of Biochemistry, Microbiology, and Immunology, Faculty of Medicine, University of Ottawa, Ottawa, ON, Canada

S. McBride · J.R. Vanstone · T. Naas · S. Redpath · H.J. McMillan · J. Brophy · H. Daoud · P. Chakraborty · D. Dyment · M. Holcik · M.A. Lines (✉)
Children's Hospital of Eastern Ontario Research Institute, Ottawa, ON, Canada
e-mail: mlines@cheo.on.ca

J. Michaud
Department of Pathology and Laboratory Medicine, Children's Hospital of Eastern Ontario and Faculty of Medicine, University of Ottawa, Ottawa, ON, Canada

T. Naas · P. Chakraborty
Newborn Screening Ontario, Ottawa, ON, Canada

Introduction

Autosomal recessive mutations of *FBXL4* (F-box and leucine-rich repeat-containing protein 4) cause a recently described form of encephalomyopathic mitochondrial DNA (mtDNA) depletion (OMIM #615471). Clinical findings in all patients described to date variably include: lactic acidosis, hyperammonemia, encephalopathy (hypotonia, microcephaly, white matter changes, and severe developmental delay), dysmorphic features, congenital cataract, and premature death in infancy or childhood (Bonnen et al. 2013; Gai et al. 2013; Huemer et al. 2015). Multiple deficiencies of respiratory chain activities are observed, with associated mtDNA depletion occurring via an unknown mechanism. Cells from patients with *FBXL4* deficiency exhibit a number of further

mitochondrial phenotypes such as reduced spare respiratory capacity and inner membrane potential, fragmentation of the mitochondrial network, and aberrant (enlarged) nucleoids. Because the function of FBXL4 and the molecular pathophysiology of this condition are unknown, a rational treatment strategy has not yet been devised, and current management is supportive.

The existing literature surrounding FBXL4 deficiency consists of only three reports (Bonnen et al. 2013; Gai et al. 2013; Huemer et al. 2015) primarily concerned with the clinical and molecular features of this rare condition. Here, we present the detailed clinical, molecular, biochemical, and bioenergetic findings in a female neonate with a homozygous *FBXL4* frameshift mutation predicted to result in a total loss of protein activity. The observed phenotype in this case, which includes hyperlactatemia, periventricular cysts, cardiomyopathy, failure to thrive, panleukopenia, profound impairment of cellular respiration, loss of inner membrane potential, altered cellular redox balance, and mitochondrial network fragmentation, demonstrates the severe and pleiotropic effects of FBXL4 deficiency on a wide range of mitochondrial functions.

Materials and Methods

Subject Recruitment and Clinical Investigations

Please refer to "Compliance with Ethical Guidelines," above, for details regarding study design and recruitment. Clinically standard investigations (conventional serum chemistries, amino acids, acylcarnitines, organic acids, histology and histochemistry, electron microscopy, spectrophotometric respiratory chain testing, and measurement of lactate to pyruvate ratio in fibroblasts) were performed on a clinical basis according to established protocols. Fibroblast cell lines were established from a small sterile skin biopsy, maintained in standard growth medium (DMEM containing 25 mM glucose, 4 mM glutamine, 10% fetal calf serum, 100 μg/ml streptomycin, and 100U/ml penicillin), and all subsequent analyses were performed at low passage (≤11) with a same-day passage-matched experimental control. Genomic analyses were carried out on whole blood lymphocyte DNA. Next-generation sequencing and mtDNA depletion studies were performed by Baylor College Medical Genetics Laboratories on a clinical basis. Microarray was performed clinically (Affymetrix CytoScan HD) according to standard protocols.

High-Resolution Respirometry

High-resolution respirometry was performed as previously described (Krumschnabel et al. 2015). Briefly, muscle was quickly transferred into ice-cold relaxation medium (BIOPS – 10 mM Ca-EGTA buffer, 0.1 μM free calcium, 20 mM imidazole, 20 mM taurine, 50 mM K-MES, 0.5 mM DTT, 6.56 mM $MgCl_2$, 5.77 mM ATP, 15 mM phosphocreatine, pH 7.1). After mechanical separation of individual fibers, chemical permeabilization was performed by agitating the fibers for 30 min in ice-cold BIOPS solution containing 50 μg/ml of saponin. Fibers were subsequently washed in ice-cold mitochondrial respiration medium (MiR05 – 0.5 mM EGTA, 3 mM $MgCl_2$, 60 mM K-lactobionate, 20 mM taurine, 10 mM KH_2PO_4, 20 mM HEPES, 110 mM sucrose, and 1 g/l BSA essentially fatty acid-free, pH 7.1), weighed, and transferred to the respirometer (Oxygraph-2k; Oroboros Instruments, Innsbruck, Austria). During the experiment, the oxygen concentration was maintained between 200 and 400 nmol/ml. Two multiple-substrate and multiple-inhibitor protocols were employed, with sequential addition of compounds into the chambers (Table 1). Data were corrected to wet weight of muscle fibers.

Micro-oximetry

Mitochondrial oxygen consumption rate (OCR) and extracellular acidification rate (ECAR) were measured in skin-derived fibroblasts as previously described (Invernizzi et al. 2012) using the Seahorse XF-24 Extracellular Flux Analyzer (Seahorse Biosciences, Massachusetts, USA). For the assessment of mitochondrial function, cells were seeded at 50,000 cells/well 1 day before the assay. On the day of the assay, growth medium was replaced with HCO_3-free DMEM containing 25 mM D-glucose, 4 mM glutamine, and 1 mM sodium pyruvate, and cells were incubated in a CO_2-free environment. Measurements of OCR were taken at 7-minute intervals following the sequential addition of 1 μg/ml oligomycin, 1 μM CCCP, and 1 μM antimycin A with 0.5 μM rotenone. All reported values for OCR are corrected to non-mitochondrial oxygen consumption as assessed after the addition of antimycin A. Data were normalized to total protein.

For the assessment of glycolytic function, cells were seeded at 50,000 cells/well 1 day before the assay. On the day of the assay, growth medium was replaced with HCO_3-free DMEM containing 143 mM sodium chloride, 3 mg/l phenol red, and 2 mM glutamine, and cells were incubated in a CO_2-free environment for 1 h. Measurements of ECAR were taken at 7-min intervals following the sequential addition of 10 mM glucose and 1 μg/ml oligomycin. All reported values for ECAR were corrected to basal ECAR as assessed before the injection of glucose (non-glycolytic acidification rate). Data were normalized to total protein.

Measurement of Glutathione and Glutathione Disulfide

Glutathione (GSH) and glutathione disulfide (GSSG) measurements were performed using a high-performance liquid chromatography (HPLC) method adapted from previously

Table 1 Mitochondrial respiration in permeabilized *vastus lateralis* fibers of patient as measured by high-resolution respirometry

Protocol 1: leak	Oxygen consumption (pmol/(s*mg))	Protocol 2: electron transport system (ETS)	Oxygen consumption (pmol/(s*mg))
Adenylate-free respiration		*Adenylate-free respiration*	
2 mM malate and 200 μM octanoyl carnitine	3.6204	2 mM malate and 5 mM pyruvate	2.0382
Fatty acid-supported respiration		*Complex I-supported respiration*	
5 mM ADP	4.8882	10 mM glutamate and 5 mM ADP	3.0307
Complex I-supported respiration		*Complex I+II-supported respiration*	
10 mM glutamate and 5 mM pyruvate	0.44885	10mM succinate (OXPHOS2)	22.2963
Complex I+II-supported respiration		*Maximal uncoupled respiration*	
10 mM succinate (OXPHOS1)	18.2139	0.25 μM titrations FCCP (chemical uncoupler)	22.6088
Leak respiration		*Complex I-independent oxygen consumption*	
2.5 μM oligomycin (ATP synthase inhibitor)	5.4048	0.5 μM rotenone (complex I inhibitor)	21.2964
Cytochrome C oxidase (COX) activity		*Cytochrome C oxidase (COX) activity*	
2 mM tetramethylphosphodinitrate (TMPD; COX-specific electron donors) and 2 mM ascorbate	49.15135	2 mM tetramethylphosphodinitrate (TMPD; COX-specific electron donors) and 2 mM ascorbate	75.4651

All values were corrected to non-mitochondrial oxygen consumption as measure by the addition of the complex III inhibitor, antimycin A (2.5 μM). $N = 1$

published work (Mailloux et al. 2012). Briefly, skin fibroblasts were collected, counted, and resuspended in a 1:1 solution of homogenization buffer (0.25 M sucrose, 3 mM EDTA, 10 mM Tris buffer, 0.1% trifluoroacetic acid, 10% methanol, pH 7.4) and acidified mobile phase (1.1% trifluoroacetic acid, 1% meta-phosphoric acid, 10% methanol). Samples were incubated (20 min, 4°C) and whole cells and cellular debris were removed by centrifugation (18,300 × *g* for 20 min at 4°C). Resulting samples were run on an Agilent Pursuit5 C18 column, and species were detected at 215 nm using a variable wavelength detector. Chromatographic peaks were integrated and total GSH and GSSG concentrations were determined. Data were normalized to cell number.

Characterization of Mitochondrial Content, Network, and Inner Membrane Potential

Patient and healthy adult control fibroblasts were plated 24–48 h prior to staining. Cells were stained with either 200 nM MitoTracker Green FM (Life Technologies, Carlsbad, CA) (for assessment of mitochondrial content) or 50 nM tetramethylrhodamine ethyl ester perchlorate (TMRE – Sigma, St. Louis, MO) (for assessment of mitochondrial inner membrane potential), trypsinized, and resuspended in PBS containing 0.2% BSA, and fluorescence was measured on a Cyan ADP 9 analyzer (Beckman Coulter, Mississauga, ON). Fluorescence signal from the autofluorescent control was subtracted from the mean fluorescence of the stained sample. For mitochondrial network visualization, cells were fixed with 4% paraformaldehyde and stained with 2 μg/ml TOMM20 (Abcam, Cambridge, UK) and 1:2000 Oregon Green (Life Technologies, Carlsbad, CA); secondary antibody was used in blocking buffer (3% BSA, 0.3% Triton X-100). Imaging was carried out by spinning disk confocal microscopy (Quorum Technologies, Guelph, ON).

Assessment of Cell Viability

Patient and control skin-derived fibroblasts were plated at 10,000–15,000 cells/well in 96-well plates. The following day, growth medium was replaced with new medium containing either 25 mM glucose or 10 mM galactose as the major carbon source, as well as 100 nM of YOYO-1 Iodide (Life Technologies, NY, USA). Measurements of cell death, as evidenced by YOYO-1 positive staining, were performed over 72 h using the IncuCyte ZOOM Live Cell Imaging System (Essen Bioscience, MI, USA). For end-point normalization, YOYO-1 positive cell counts were expressed as a fraction of the total number of cells.

Results

The subject, a female neonate, was born to a *gravida* 3, *para* 2 French Canadian mother, and an unidentified but reportedly nonconsanguineous father, following a term pregnancy notable only for diet-controlled gestational diabetes. The delivery was uneventful, with Apgar scores

of 8 at 1 min and 9 at 5 min. Birth weight was 2,620 g (8th centile). The initial presenting symptom was temperature instability at 12 h of age. Laboratory studies at that time showed a marked metabolic acidosis (pH 7.13; pCO2 16 mmHg; HCO_3^- 5 mmol/l; base excess –21.6 mmol/l). MRI of the brain at 1 day of age (Fig. 1a–c) showed diffuse T2 hyperintensity of the supratentorial white matter, consistent with edema, bilateral enlargement of the lateral ventricles with bilateral intraventricular and periventricular cysts as well as absent myelination of the posterior limb of the internal capsule. MR spectroscopy (TE 144) identified a lactate doublet in the basal ganglia. Echocardiography and Holter monitor showed signs consistent with suprasystemic pulmonary hypertension and atrial ectopic tachycardia, requiring treatment with flecainide. Given the working clinical diagnosis of a mitochondrial disorder, a number of biochemical and genomic investigations were undertaken, as detailed below, and the patient was started on cofactor therapy with (variously) carnitine, riboflavin, ubiquinone, biotin, and thiamine, to no obvious beneficial effect. She remained in NICU until two months of age. At four months of age, the subject's examination revealed hypotonia and dysmorphic features (Fig. 1d). By seven months of age, chronic failure to thrive, requiring chronic nasogastric feeding, was apparent, along with evidence of immunodeficiency comprising neutropenia, pan-lymphopenia, and

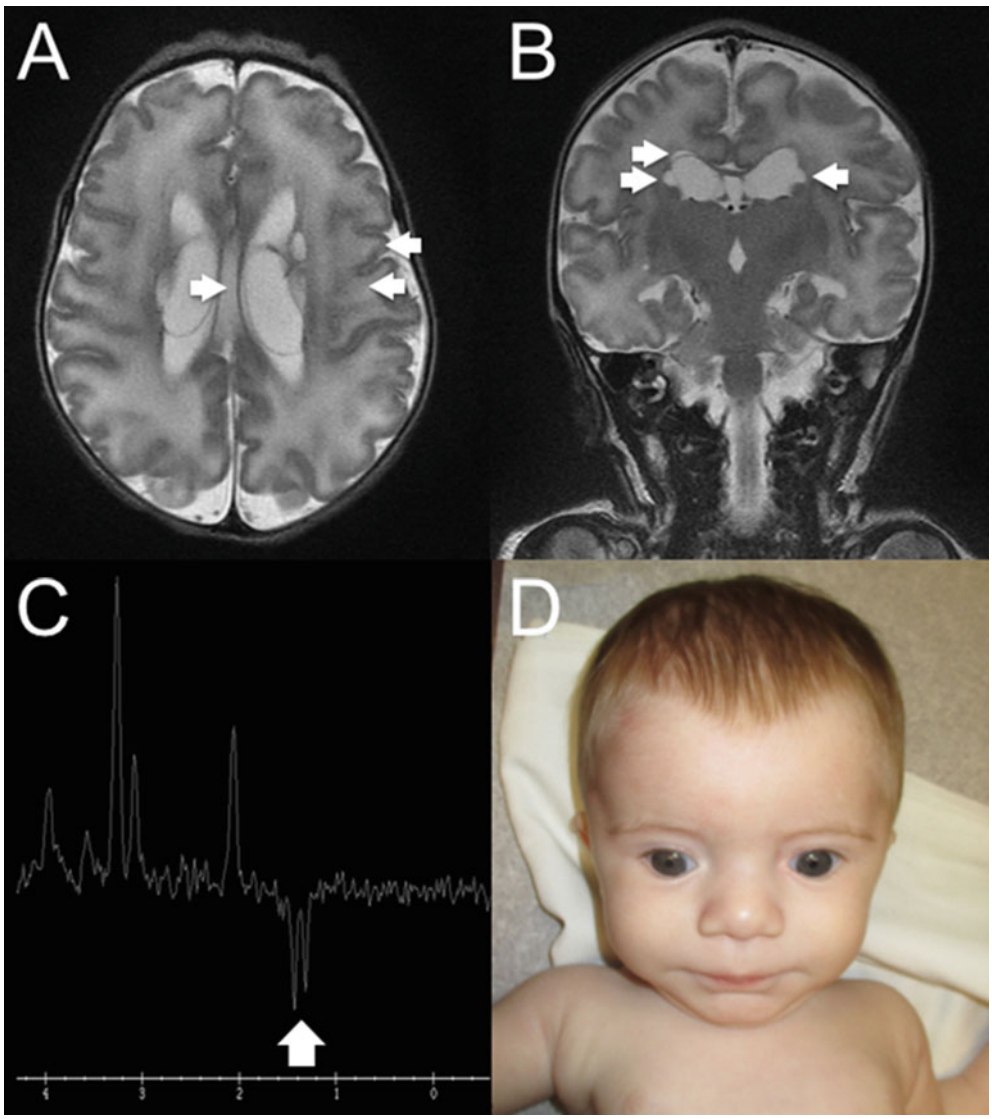

Fig. 1 Cranial MRI at five days of age showed (**a**, **b**) diffuse white matter edema with bilateral intra- and periventricular cysts, a single right occipital focus of restricted diffusion likely related to focal ischemia (not shown), and (**c**) a large lactate doublet in the left basal ganglia by MR spectroscopy. Craniofacial morphology (**d**) was notable for midface hypoplasia, short palpebral fissures, and lightly grooved philtrum. The presenting clinical features were considered to be consistent with a mitochondrial disease and/or pyruvate dehydrogenase deficiency

hypogammaglobulinemia. This presented with severe oral thrush and *Pneumocystis jirovecii* prophylaxis was initiated. Now 14 months old, she remains hypotonic and globally delayed, with milestones equivalent to a four-month-old. Immunoglobulins and neutrophil numbers improved with time and improved nutrition via NG tube feeding; further lymphocyte evaluation is underway.

Biochemical findings in the patient include: lactate, initially 21.6 mmol/l, decreased to 4.3 mmol/l by day 3 of life, and has remained elevated, 3–15 mmol/l; a normal blood lactate concentration has never been recorded in this child. Plasma amino acids showed consistently increased alanine (565–1,086 μmol/l; ref. 143–439 μmol/l), proline (286–515 μmol/l; ref. 52–298 μmol/l), and serine (227–274 μmol/l; ref. 71–186 μmol/l). Acylcarnitine profile showed diffuse elevations in short-, medium-, and long-chain acylcarnitines and acetylcarnitine and small amounts of propionylcarnitine. Urine organic acids (several occasions) have variously showed lactic, pyruvic, and ethylmalonic acids, ketone bodies, Krebs cycle intermediates, and (inconsistently) branched-chain alpha-ketoacids. A *vastus lateralis* biopsy (Supplemental Fig. 1; Supplemental Table 1) obtained at one month of age showed increased lipid droplets and intrasarcoplasmic glycogen, with deficiency of all respiratory chain activities, and particularly of cytochrome oxidase. Ultrastructurally, the mitochondria were fewer in number, some of which are larger and dysmorphic (Supplemental Fig. 1).

Genetic investigations in the patient were as follows: despite no known parental consanguinity, SNP microarray showed a single ~27 Mb region of copy-neutral loss of heterozygosity on chromosome 6 (arr[hg19] 6q13q16.3 (73958441-100963633)x2 hmz). Next-generation sequencing of a combined nuclear and mtDNA panel showed a homozygous frameshift, c.1641_1642delTG (p.C547*), in the gene *FBXL4*, which resides within the 6q marker homozygosity block. This variant has been detected 18 times in 121,202 exomes (allele frequency 0.015%) in the Exome Aggregation Consortium dataset (ExAC, Cambridge, MA, http://exac.broadinstitute.org; accessed July 2015). mtDNA copy number in skeletal muscle in the patient was 37% of control, consistent with mtDNA depletion.

To better delineate the mitochondrial pathophysiology of FBXL4 deficiency, a battery of bioenergetic studies in patient tissues and cells was next conducted. High-resolution respirometry of saponin-permeabilized muscle fibers (Table 1) showed very little respiration on complex I-, complex II-, or ETF-linked substrates. Although this analysis was hindered by the lack of a matched pediatric control specimen, we did observe that (i) all measured rates were very low (<1/3 of published healthy adult reference values) (Gnaiger 2009; authors' unpublished data), and (ii) the addition of rotenone, a complex I inhibitor, had no demonstrable effect on respiration rates, implying a near-complete absence of complex I-linked respiration. Micro-oximetry of patient fibroblasts showed reductions in oxygen consumption rate (OCR) at rest (Fig. 2a) and when stimulated with the inner membrane protonophore carbonyl cyanide m-chlorophenylhydrazone (CCCP) (maximal respiration) (Fig. 2d). This corresponded with reductions in both complex V-coupled ("phosphorylating") and uncoupled ("leak") respiration in the same assay (Fig. 2b). In contrast, the glucose- and oligomycin-stimulated extracellular acidification rate (ECAR, an indirect measure of glycolytic activity) in the cells was enhanced (Fig. 2e, f), suggesting a corresponding overreliance on glycolysis relative to oxidative phosphorylation (Fig. 2g).

The effects of the subject's profound respiratory chain defect on the mitochondrial network and cellular stress responses were further investigated. Spinning disk confocal microscopy of fixed fibroblasts immunostained for the outer membrane transporter TOMM20 (Fig. 3a) confirmed fragmentation of the mitochondrial network. Assessment of mitochondrial content and inner membrane charge in live patient fibroblasts using flow cytometric staining of the cationic lipophilic dyes MitoTracker Green and TMRE showed a reduction in inner membrane potential (Fig. 3b) with no demonstrable difference in mitochondrial content (Fig. 3c).

Assessment of cell viability by time-lapse video microscopy under normal growth conditions (Fig. 3d) showed reduced viability of patient versus control fibroblasts. This phenotype was exacerbated under mandatory aerobic respiration in a medium containing galactose as the principal energy substrate and was most apparent after 72 h (Fig. 3e). HPLC determination of glutathione (GSH) and glutathione disulfide (GSSG) in fibroblasts (Fig. 3f) showed evidence of altered redox poise, more specifically, lower levels of reduced glutathione (GSH) ($p = 0.049$) and an abnormally low GSH:GSSG ratio ($p = 0.00018$).

Discussion

We identified a homozygous frameshift mutation in *FBXL4* in a neonate with a severe mitochondrial phenotype comprising lactic acidosis, CNS, cardiac, and bone marrow involvement, and multicomplex respiratory chain dysfunction associated with mtDNA depletion. Cells from the patient exhibited profoundly deficient respiration of complex I-, II-, and ETF-linked substrates, with loss of inner mitochondrial membrane potential, mitochondrial network fragmentation, and increased cell death under obligate respiration on galactose medium. Cellular glutathione redox poise was also abnormal in patient cells, characterized by a more oxidized cellular milieu. With the exception of mitochondrial mass as assessed by flow cytometry, all other aspects of mitochondrial function were

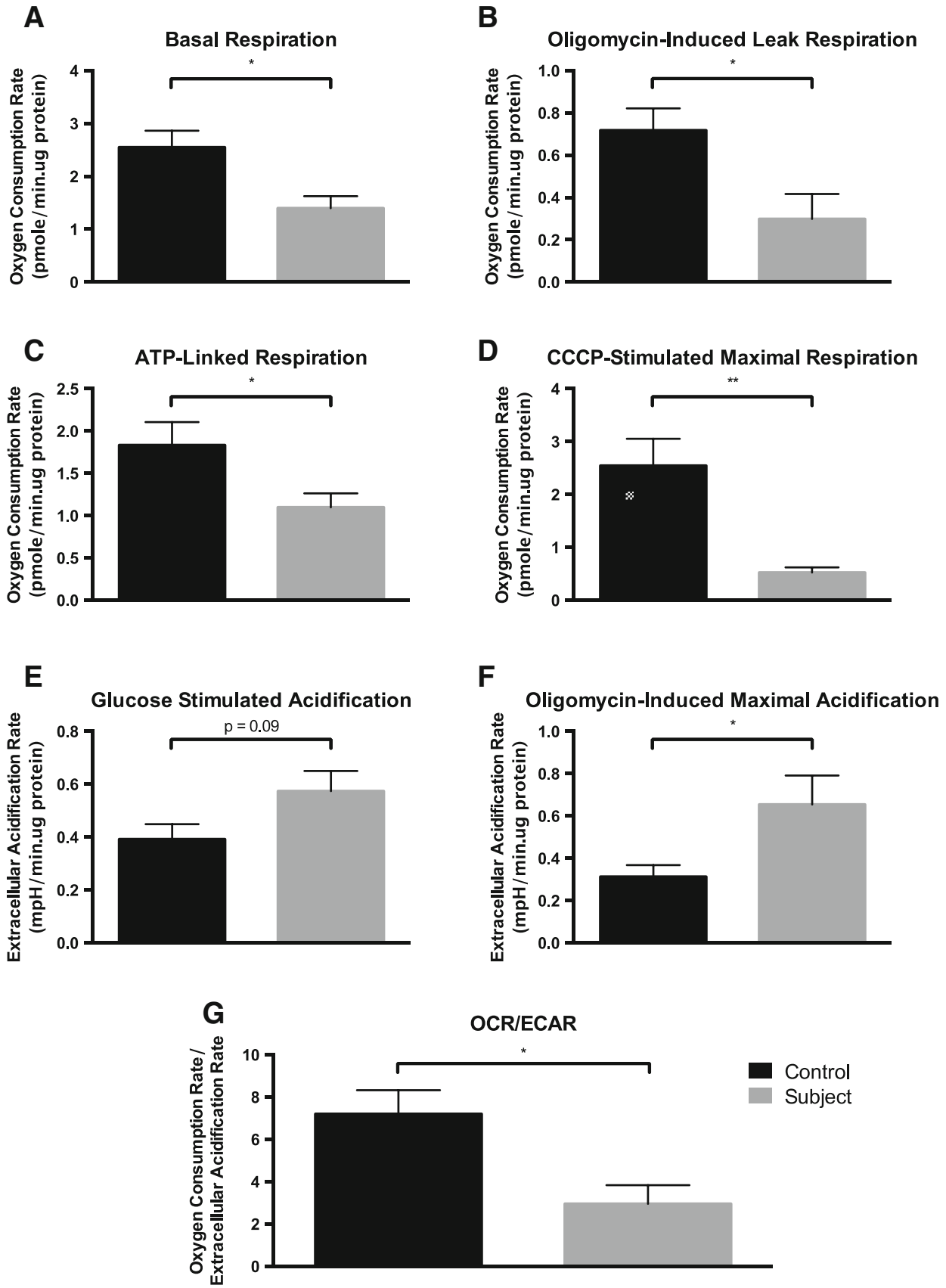

Fig. 2 Assessment of respiratory parameters in skin-derived fibroblasts by micro-oximetry. (**a**–**d**) Oxygen consumption rate (OCR) in patient and control fibroblasts in the presence of glucose, pyruvate, and glutamine. Values are corrected to non-mitochondrial OCR persisting after addition of antimycin A and rotenone. (**a**) Basal OCR. (**b**) Leak OCR measured following inhibition of complex V by

markedly abnormal, i.e., deficiency of FBXL4 had severe and pleiotropic effects on mitochondrial function. As our proband's homozygous frameshift is predicted to completely abolish FBXL4's expression, the phenotype in our patient is likely situated at the severe end of the *FBXL4* clinical spectrum. Of note, our patient did not manifest hyperammonemia, as described in a proportion of the previously described cases. Considering the few other reported individuals with two severe (truncating) *FBXL4* mutations (Huemer et al. 2015, patients 2, 3, 11, 12, 13), no clinical features can currently be consistently associated with total FBXL4 deficiency. However, some reported manifestations include craniofacial abnormalities, immune system deficiencies as well as congenital cataracts and hypoplastic cerebella.

As previously reported, (Bonnen et al. 2013; Gai et al. 2013) our micro-oximetry experiments in patient fibroblasts showed a deficiency of both basal and maximally stimulated respiration, with a simultaneous overreliance on glycolysis as approximated by ECAR. Of note, the standard clinical fibroblast lactate to pyruvate ratio in this patient was only slightly elevated (27.6) despite the patient's marked permanent hyperlactatemia and hyperalaninemia, and on this occasion micro-oximetry appeared to offer a more faithful demonstration of the patient's respiratory phenotype in cells.

A novel finding of our study is that fibroblasts from our patient exhibited a more oxidized GSH:GSSG ratio, reflecting a perturbation of glutathione-dependant redox poise. This could be caused by either an increase in reactive oxygen species (ROS) production and/or a decrease in ROS quenching capacity (Mailloux et al. 2013a). Because protein glutathionylation is known to affect the activity of various respiratory chain proteins and uncoupling proteins including UCP3 (Mailloux et al. 2013b), altered redox status could potentially have knock-on effects on the regulation of protein glutathionylation and on the glutathionylation of energy substrates such as fumarate (Sullivan et al. 2013). The potential role of excessive oxidative stress on the reduced cellular survival observed in the proband's cells under mandatory respiration requires confirmation as does the exploration of any effect of cofactor, drug, and/or antioxidant "therapy" on patient cells in vitro.

Very little is known about the actual molecular pathogenesis of FBXL4 deficiency. FBXL4 belongs to a family of leucine-rich repeat (LRR)-containing F-box proteins, other members of which are adaptor subunits of multiprotein complexes with specific (phosphorylation-dependent) E3 ubiquitin ligase activity (Skowyra et al. 1997). FBXL4, which localizes to the mitochondrial intermembrane space and participates in a 400 kDa quaternary complex, is hypothesized (but not proven) to have a similar activity. In addition, a role in mitochondrial quality control similar to the PINK1-dependent recruitment of parkin, another E3 ubiquitin ligase, has been proposed (Gai et al. 2013). If true, this model would imply that the mtDNA depletion seen in FBXL4 deficiency is secondary to altered mitophagy, mitochondrial dynamics, and/or quality control; however, apart from the relatively nonspecific observation that the mitochondrial network is fragmented in FBXL4 deficiency, this model has not yet been tested experimentally.

An effective therapeutic approach for FBXL4 deficiency is clearly wanting. Of the three available inputs to the respiratory chain, complex II-linked respiration appears to be the least profoundly impaired, at least in our patient, whereas oxidation of NADH-linked substrates appears to be poor. Empiric cofactor therapy with riboflavin, biotin, thiamine, pyridoxine, coenzyme Q, and (briefly) carnitine appears to have had no beneficial effect in our patient. We would add the important caveat that children with this condition should be evaluated for immune system dysfunction, and live vaccinations be withheld if appropriate. Patient fibroblasts, which display several "screenable" phenotypes in FBXL4 deficiency, may serve as a useful model in which to study the pathobiology of this condition, as well as its response to drugs and other pharmacologic agents.

Conclusions

Total FBXL4 deficiency in our patient was characterized clinically by severe multisystem disease including lactic acidosis, cystic white matter lesions, cardiomyopathy, arrhythmias, and immunodeficiency. The main physiological findings in cells from this patient include profound reductions in complex I-, II- and ETF-linked substrate-dependant respiration, a loss of inner membrane potential, and fragmentation of the mitochondrial network with no parallel decrease in mitochondrial content. A novel finding of this study was the marked glutathione oxidation in our patient's cells, suggesting either a failure of endogenous antioxidant defenses or increased ROS generation. We propose that cultured patient cells may serve as a convenient model in which to preclinically evaluate potential drug and/or cofactor therapies for this rare but increasingly recognized mitochondriopathy.

Fig. 2 (continued) oligomycin. (**c**) Phosphorylation-coupled OCR, estimated as the resulting decrease in OCR after oligomycin. (**e**, **f**) Extracellular acidification rate (ECAR), an indirect measure of glycolytic activity in cells. Rates are corrected to non-glycolytic acidification rate as measured prior to the addition of glucose. (**e**) Glucose-stimulated ECAR. (**f**) Maximal (oligomycin-stimulated) ECAR. (**g**) Ratio of basal OCR to glucose-stimulated ECAR. $N = 6$. Values are presented as mean ± SEM; $*p < 0.05$, $**p < 0.01$ analyzed by unpaired, two-tailed Student's *t*-test

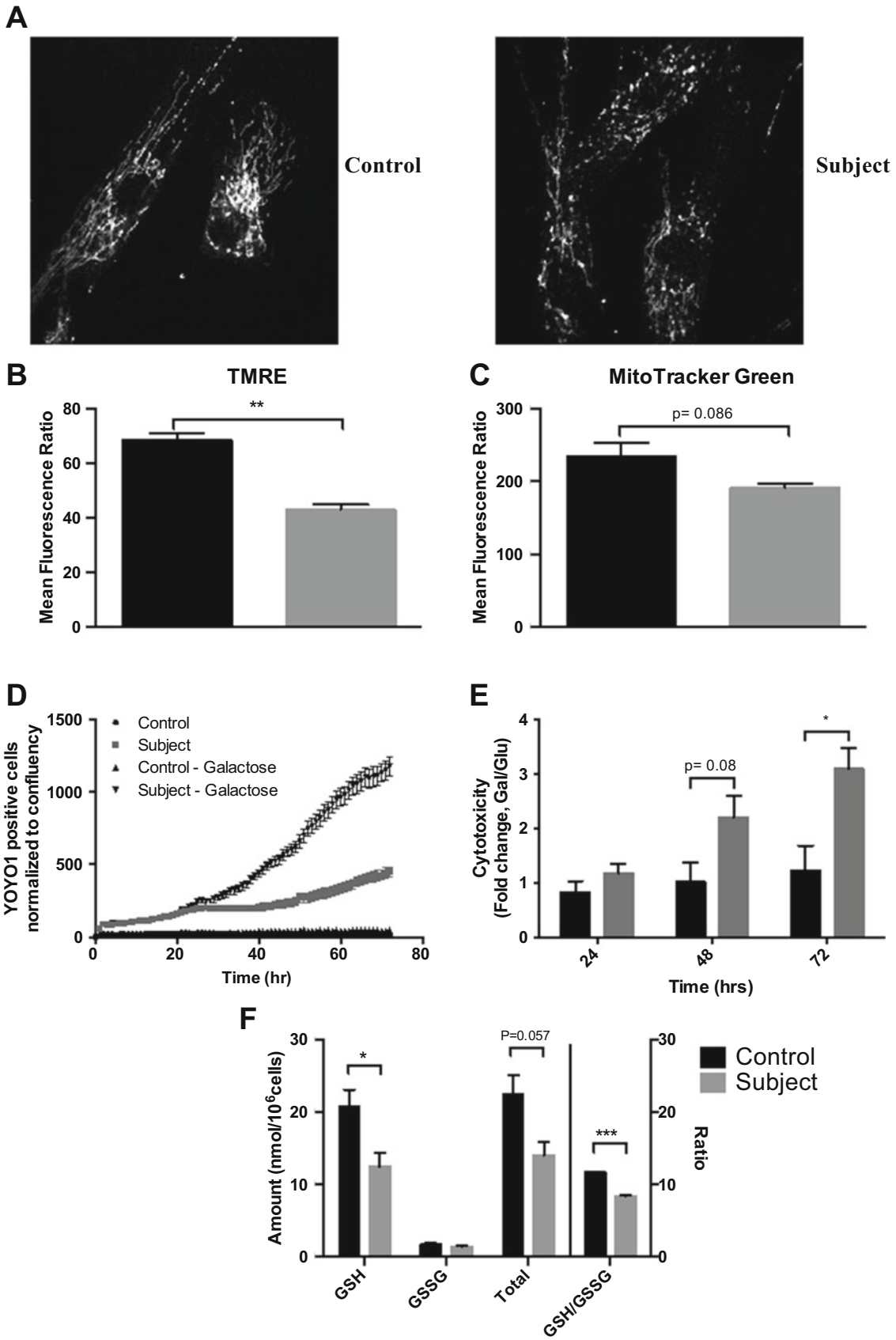

Fig. 3 Assessment of mitochondrial content, inner membrane potential, and network branching by cell staining in skin-derived fibroblasts. (**a**) Spinning disk confocal microscopy of fixed control (*left*) and patient (*right*) fibroblasts immunostained for the outer membrane transporter TOMM20. (**b**) Mitochondrial content (MitoTracker Green) ($N = 3$) and (**c**) inner membrane potential (TMRE)

One Sentence Summary

A homozygous frameshift mutation in *FBXL4* was identified in a neonate with primary lactic acidosis, in whom cell-based mitochondrial phenotyping demonstrated severe global mitochondrial dysfunction.

Compliance with Ethics Guidelines

Conflict of Interest

Ghadi Antoun, Skye McBride, Jason R. Vanstone, Turaya Naas, Jean Michaud, Stephanie Redpath, Hugh J. McMillan, Jason Brophy, Hussein Daoud, Pranesh Chakraborty, David Dyment, Martin Holcik, Mary-Ellen Harper, and Matthew A. Lines declare that they have no conflict of interest.

Informed Consent

All procedures followed were in accordance with the Tri-Council Policy Statement: Ethical Conduct for Research Involving Humans (2010) and with the Helsinki Declaration of 1975, as revised in 2000. Informed consent was obtained from all patients participating in the study. The research protocol was approved by the Children's Hospital of Eastern Ontario Research Ethics Board.

Authors' Contributions

All authors contributed to the conception and design of the study. ML, SR, JM, HJM, and JB acquired the clinical and genomic data. GA, SM, JV, and TN generated respirometry and cell-based data for mitochondrial phenotyping. Data were analyzed and interpreted by GA, SM, JV, TN, JM, MEH, and ML. The manuscript was drafted by GA, SM, MEH, and ML. Critical revisions were performed by all authors.

References

Bonnen PE, Yarham JW, Besse A et al (2013) Mutations in FBXL4 cause mitochondrial encephalopathy and a disorder of mitochondrial DNA maintenance. Am J Hum Genet 93:471–481

Gai X, Ghezzi D, Johnson MA et al (2013) Mutations in FBXL4, encoding a mitochondrial protein, cause early-onset mitochondrial encephalomyopathy. Am J Hum Genet 93:482–495

Gnaiger E (2009) Capacity of oxidative phosphorylation in human skeletal muscle: new perspectives of mitochondrial physiology. Int J Biochem Cell Biol 41:1837–1845

Huemer M, Karall D, Schossig A, et al (2015) Clinical, morphological, biochemical, imaging and outcome parameters in 21 individuals with mitochondrial maintenance defect related to FBXL4 mutations. J Inherit Metab Dis

Invernizzi F, D'Amato I, Jensen P, Ravaglia S, Zeviani M, Tiranti V (2012) Microscale oxygraphy reveals OXPHOS impairment in MRC mutant cells. Mitochondrion 12:328–335

Krumschnabel G, Fontana-Ayoub M, Sumbalova Z et al (2015) Simultaneous high-resolution measurement of mitochondrial respiration and hydrogen peroxide production. Methods Mol Biol (Clifton, NJ) 1264:245–261

Mailloux RJ, Adjeitey CN, Xuan JY, Harper ME (2012) Crucial yet divergent roles of mitochondrial redox state in skeletal muscle vs. brown adipose tissue energetics. FASEB J 26:363–375

Mailloux RJ, McBride SL, Harper ME (2013a) Unearthing the secrets of mitochondrial ROS and glutathione in bioenergetics. Trends Biochem Sci 38:592–602

Mailloux RJ, Xuan JY, Beauchamp B, Jui L, Lou M, Harper ME (2013b) Glutaredoxin-2 is required to control proton leak through uncoupling protein-3. J Biol Chem 288:8365–8379

Skowyra D, Craig KL, Tyers M, Elledge SJ, Harper JW (1997) F-box proteins are receptors that recruit phosphorylated substrates to the SCF ubiquitin-ligase complex. Cell 91:209–219

Sullivan LB, Martinez-Garcia E, Nguyen H et al (2013) The proto-oncometabolite fumarate binds glutathione to amplify ROS-dependent signaling. Mol Cell 51:236–248

Fig. 3 (continued) ($N = 3$) were measured by flow cytometry. Values are presented as mean ± SEM; $^{**}p < 0.01$ analyzed by unpaired, two-tailed Student's *t*-test. (**d**) Time course of patient and control fibroblasts showing increased cell death (as evidenced by YOYO1-positivity) of patient cells versus control cells. (**e**) This difference is magnified when cells are grown under mandatory respiration in galactose-containing medium after 72 h. $N = 3$. Values are presented as mean ± SEM; $^{*}p < 0.05$ analyzed by unpaired, two-tailed Student's *t*-test. (**f**) Levels of glutathione (GSH) and glutathione disulfide (GSSG) from skin-derived fibroblasts of control and subject. Values are corrected to cell number. $N = 3$. Values are presented as mean ± SEM; $^{*}p < 0.05$, $^{***}p < 0.001$ analyzed by unpaired, two-tailed Student's *t*-test